The Notch and EGFR signaling regulate caspase inhibitor Diap1 to match supply with intestinal demand

Tobias Reiff[1,2,†], Zeus Antonello[1,3,†], Esther Ballesta-Illán[1], Laura Mira[1], Salvador Sala[1], Maria Navarro[1], Luis M. Martinez[1], Maria Dominguez[1,4]

[1]Instituto de Neurociencias, Consejo Superior de Investigaciones Científicas-Universidad Miguel Hernández (CSIC-UMH), Avda Santiago Ramón y Cajal s/n, Campus de Sant Joan, Alicante, Spain

[2] Present address: Institute of Genetics, Heinrich-Heine-University, Universitätsstr. 1, Düsseldorf, Germany

[3]Present address: Department of Surgery, Division of Surgical Research, Cooper University Hospital, Camden, New Jersey, USA.

[4]Author for correspondence: Maria Domínguez, Instituto de Neurociencias, E-mail: m.dominguez@umh.es,

[†]These authors contributed equally

Running title: Diap1 in intestinal homeostasis

Highlights

- Steady-state intestinal stem cell's production involves programmed cell death
- Survival or death of enteroblasts is controlled by balance of pro-apoptotic and antiapoptotic signals impinging on Death-associated inhibitor of apoptosis 1 (Diap1)
- Opposite activity of Notch (N) and EGFR activation in enteroblasts controls the death/life decision
- Lozenge/Runx and Klumpfuss/WT1 in enteroblast mediates cell death and differentiation

Summary

The regenerative activity of adult stem cells carries a high risk of cancer, particularly in highly renewable tissues. To guarantee that the correct organ size is attained and to cope with the continual risk of cancer, developing tissues often use programmed cell death (PCD) as an adaptive mechanism to cull excess and abnormal cells. Members of the family of Inhibitor of Apoptosis Proteins (IAPs) inhibit caspases and cell death and are often overexpressed in cancer. Here, we show that *Diap1* is expressed in committed progenitor (enteroblast) cells in the adult *Drosophila* intestine. Blocking endogenous caspases uncovered that more than half of enteroblasts produced by intestinal stem cells (ISCs) are actively eliminated by apoptosis in the physiological intestine and also led to tumorigenesis. We find that antagonistic interplay between the Notch and EGFR signaling on Diap1 regulation governs the enteroblast cell death or survival decision via the conserved Klumpfuss/WT1-Lozenge/RUNX axis, which also regulates of differentiation plasticity of enteroblasts. These data provide new insights into how apoptosis drives adult tissue renewal and protection against tumors.

Introduction

The *Drosophila* intestinal epithelium is renewed completely several times over its 40-50 day adult life in a process that takes one to three weeks under normal homeostatic self-renewal (Antonello et al., 2015; Jiang et al., 2009; Ohlstein and Spradling, 2007). However, after an overt damage, it is renewed in just two-three days (Buchon et al., 2009; Jiang et al., 2009; Ohlstein and Spradling, 2007). The wide range of physiological turnover time reflects the stochastic damage of absorptive enterocytes (ECs), the main cells in the intestinal epithelium (Biteau et al., 2011; Jiang and Edgar, 2011), by exposure to pathogens and toxins present in food and chemical and physical stress, and the adaptive capacity of the intestine. The intestine also contains secretory enteroendocrine (EE) cells, which constitute only 10% of the intestinal population and renew themselves at a slower rate than ECs (de Navascués et al., 2012; Sallé et al., 2017; Parasram et al. 2018). Intestinal cell turnover is sustained by a small population of ISCs scattered throughout the epithelium that, as observed in other high turnover epithelia in mammals (Simons and Clevers, 2011), divide regularly and produce, with each division, one cell that differentiates and one that remains undifferentiated and will divide in the same way to produce a new cell stem and a cell committed towards the same lineage as the previous division or into the other intestinal cell type (e.g. Jiang et al., 2009; Micchelli and Perrimon, 2006; Ohlstein and Spradling, 2006; 2007). ISCs can also divide symmetrically (de Navascués et al., 2012; O'Brien et al., 2011) and directly differentiate into EE without division (Zeng and Hou, 2015). However, in the highly renewing intestine, stem cells must operate rapidly and efficiently by providing enough new cells to replenish daily tissue demand. Moreover, since multipotent ISCs have different options in terms of cell lineage, an outstanding open question is how individual stem cells rapidly and adaptively produce the distinct tissue cell types at the right number to sustain tissue homeostasis in short- and long-term.

In *Drosophila,* ISCs are the only mitotic cells and their immediate committed progeny, enteroblasts (EBs), terminally differentiate without further division into only two possible cell types (EC or EE) through differential Delta (Dl)-Notch (N) activation in the daughter cell that become the committed progenetitor cell (Ohlstein and Spradling, 2007; Perdigoto et al. 2011). These features of the adult fly gut simplify the analysis of the dynamics of ISC production during homeostasis. *Drosophila* ISCs divide slowly but continually and produce EBs that can remain incompletely differentiated for long periods in the absence of a local (Antonello et al., 2015). The existence of such a pool of EBs in homeostatic

intestines was first suggested in studies of infection challenge (Buchon et al., 2009) but only formally established by multicolour tracing methods (Antonello et al., 2015). After infection, or genetic induction of enterocyte death (Buchon et al., 2009; Jiang et al., 2009), the ISC proliferation rate increases to cope with the increased demand for new cells. The mitotic index can increase from 3 to 5 mitosis *per* midgut to more than 100 mitosis *per* gut, however, ISC proliferation rate peaks only 24-48 hours *post* challenge (Buchon et al., 2009; Jiang et al., 2009). During the time interval between challenge and the raise of ISC proliferation, it has been shown that the 'pre-existing' EB pool serves as the intestine's first defence (Buchon et al., 2009; Antonello et al., 2015). A fundamental question is how the stem cell population performs in times of low intestinal demand since maintaining an 'unnecessary' population of immature EBs may increase work load and metabolic demand and thus lead to poorer organ performance or risk of tissue hyperplasia (Zhai et al., 2015).

Developing organs often use a strategy of overproduction followed by culling of the excess cells via programmed cell death (PCD) to ensure correct organ size and shape (Fuchs and Steller, 2011). Although counterintuitive that adult stem cells overproduce (i.e. divide superfluous), here we discovered that ISCs divide in greatly excess to physiological demand and cull excess enteroblast cells via a PCD similar to those operating during morphogenesis. We found Dl-induced N activation primes enterocyte-committed progenitor cells to death via the pro-apoptotic transcription factor Klumpfuss/WT, which also regulates fate diversification. Excecution of cell death involves activation the RUNX homologue Lozenge and is counteracted by environmental survival signals acting via the Epidermal Growth Factor Recepto (EGFR) in enteroblast cells, impinging on regulation of the caspase inhibitor DIAP1. Loss of *diap1* resulted in complete loss of enteroblast and abrogation of intestinal renewal, whereas blocking caspase genes uncovered that more than half of the enterocyte-committed progenitor cells produced by the ISCs are eliminated by PCD in the physiological intestine in conditions of low demand. In addition, selective elimination of apoptosis in progenitor cells is sufficient for tumorigenesis to occur. These data provide new insights into the contribution of programmed cell death in adult tissue homeostasis, opening new avenues for future investigation of intestinal cancer.

RESULTS

Intestinal Stem Cells Do not Adjust their Division to Slowing Intestinal Cell Replacement

In order to test whether ISCs division adapt to situations of low demand, we developed a 'Low demand' protocol to minimize the need for intestinal cell replacement (Figure 1A). The key features of our protocol to assess ISC's production that differentiate from previously studies are: first, to minimize changes of pathogens accumulation in the food, which is the leading cause of EC damage (Apidianakis and Rahme, 2010), we frequently transferred flies to fresh food vials (i.e. 3-4 days old flies were transferred to fresh food vials every 48 hour: Figure 1A). Second, we used our tracing method ReDDM ('Repressible Dual Differential Marker': Antonello et al., 2015), which allows to trace differentially stem and progenitor cells and the differentiated progeny (Figure 1B). New ECs are detected as RFP-only cells by the ReDDM tracing method (Figure 1B), whereas ISCs and/or EBs are detected as double GFP-RFP-labelled cells. Control flies were transferred to fresh vials every week as previously reported (Antonello et al. 2015; Jian et al., 2009) and as expected from unpredictable fluctuating demands, there was increased renewal of ECs and substantial variation among individual midguts (Figure 1C, pattern histogram). This widely used standard culturing condition will refer to as 'Variable' demand. In 'Low' demand, few EC had renewed at day 7, 14 and even 21 after tracer induction (esg^{ReDDM}-midgut; Figure 1C, solid histogram) compared with control gut in normal culturing condition (new food vial every week) where the intestinal epithelium had renewed completely after three weeks (Figure 1C), as previously reported (Antonello et al., 2015; Jiang et al., 2009). In spite of the slow epithelial cell turnover in 'Low demand' condition, ISCs continued dividing at the same rate that midguts reared in normal culturing conditions (Figure 1D). $PH3^{+}$ counts showed that ISCs in 'Low demand' maintained a constant proliferation rate (2-5 mitosis/midgut) at day 7, 14 and 21 (Figure 1D). Representative images of guts reared at the standard condition (refered as variable demand) and the low demand condition are in Figure 1E-G. No accumulation of EBs was observed in 'Low' midguts after three weeks of continued ISC division (Figure 1G). This could not be attributed to terminal differentiation because the ReDDM tracing method detected very few renewed ECs (RFP-only labelled cells reflect the newly renewed ECs, Figure 1F-G). Prompted by this observation, we next investigated directly whether stem cell production might be regulated by a PCD.

Blocking Apoptosis Selectively in ISCs and Enteroblasts Led to Accumulation of Undifferentiated Progenitor Cells and Tumor Masses

We first drove in age-synchronized cohorts of adult flies the expression of the baculovirus caspase inhibitor *p35* in ISCs and EBs using esg^{ReDDM} system and found a significant accumulation of *esg*-positive (*esg*+ve) cells after 7 days of *p35* expression (esg^{ReDDM}>*p35*: compare with control Figure 1H and I) and the occasional presence of tumour-like masses (Figure 1J). This evidenced that ISCs produce in excess to demand uncovered a role of caspases in controlling stem and/or progenitor cell number. We next used the caspase sensor Apoliner that allows the detection of an even rarer number of apoptotic cells because it marks early steps of apoptosis while the cell still appears morphologically normal (Bardet et al., 2008). To distinguish from apoptosis induced in aging or damaged ECs and EEs, we drove *Apoliner* specifically in ISC and EBs using *esg-Gal4* and in this way we mapped caspase activity within the EB population (Figure S1A-C). This provides a first hint that apoptosis occurs in EB population. This notion is reinforced later by functional studies, and analysis of apoptosis using TUNEL (Terminal Deoxynucleotidyl Transferase (TdT)-mediated dUTP Nick-End Labelling; see below).

Endogenous Diap1 in Enteroblast Counterbalances Caspase-Induced Enteroblast Death

Diap1 protein (Vasudevan and Ryoo, 2015) is crucial for inhibition of caspases (Meier et al., 2000) and, consistent with above observations, we found that the Diap1 transcriptional reporter *Diap1-GFP* (Djiane et al., 2013; Zhang et al., 2008) is selectively expressed in EB cells (Figure 1K). *Diap1-GFP* co-localized with the N-activity-reporter (*GBE-Su(H)-lacZ*; Figure S1D), which is commonly used to label EBs (Furriols and Bray, 2000; Micchelli and Perrimon, 2006; Zacharioudaki and Bray, 2014). *Diap1*-expressing cells were negative for ISC marker Delta (Dl) (Figure S1D), PH3 (inset Figure 1K) and for EE marker Prospero (Pros: Figure 1L and M). These analyses revealed that EBs but not ISCs expressed *Diap1*.

The pro-apoptotic proteins Reaper (Rpr), Head involution defective (Hid) and Grim regulate most apoptotic deaths by counteracting Diap1 (Hirata et al., 1995; Holley et al., 2002; Meier et al., 2000) (Figure 2A). The *H99* deficiency removes these pro-apoptotic genes (Fuchs and Chen, 2013) and the adult intestine of flies heterozygous for *Df(3L)H99* had a two-fold increase in number of EB (Figure 2B and C) as determined by counting *Diap1-GFP* cells (Figure 2D), consistent with apoptosis-mediated culling of EBs being a physiological process. Importantly, in *Df(3L)H99* heterozygous flies, many EBs show reduced expression levels of *Diap1* compared with control guts, as suggested by the reduction of fluorescence intensity of the reporter (Figure 2B, C and E). One interpretation of this finding is that EBs

with low Diap1 can survivel when gene dosage of of pro-apoptotic genes is reduced. This would suggest that survival of an enteroblast might depend on the balance between survival and apoptotic inputs.

To investigate the dynamics of PCD in regulating EB number without perturbing ISCs, we then used a Gal4 enhancer trap in *klu* gene, encoding the *Drosophila* Wilms' Tumour 1 homologue (Klein and Campos-Ortega, 1997), which we found drives expression selectively in EBs (Figure S1E and F). Lineage tracing of *klu-Gal4* (*klu*$^{+}$) cells using ReDDM showed all differentiated cells derived from *klu*$^{+}$ EB cells are ECs and none of them are destined to EE fate (Figure S1F-H).

We assayed adult- and EB-selective RNA interference (RNAi)-based silencing of the caspases *Debcl* (Death executioner Bcl-2), *Dark* (Death-associated APAF1-related killer), *Dredd* (Death related ced-3/Nedd2-like caspase) and *Drice* (Death related ICE-like caspase) (Figure 2F-H and Figure S2A-C), using *klu*^{ReDDM} in 'Low demand' culturing condition. At day 7 after RNAi transgene induction and tracing, we observed a more than two-fold accumulation of EBs (Figure 2F-H and quantification of *Debcl-RNAi* in J) and the effect could not be accounted for defects in intestinal cells renewal since new ECs (single RFP^{+} cells) were present in similar number or higher than controls (Figure 2F-H and quantification in K). Together these data support that significant numbers of EBs are culled by a caspase-dependent apoptosis in adult homeostatic guts.

RNAi silencing of the caspase inhibitor *Diap1* in EBs (Figure 2I), and the overexpression of its target the caspase *Dronc* (Meier et al., 2000) (Figure S2D-E), led to the elimination of most *klu*$^{+}$ cells. To monitor apoptotic cells under conditions of expression of RNAi transgenes silencing apoptotic factors, and the *Diap1-RNAi*, we used the TUNEL assay, which detects extensive DNA degradation (late stages of apoptosis). TUNEL method led to strong decay of fluorescent reporters and we could only identify progenitors marked by GFP using the stronger Gal4 driver, *esg-Gal4* (Ohlstein and Spradling, 2006) but not using *klu-Gal4* or *Su(H)-Gal4*.

Silencing of the caspases *Debcl* and *Drice* using *esg-Gal4* were accompanied by a decrease in the number of apoptotic *esg*-positive *(esg*$^{+}$*-ve)* cells, while silencing *Diap1* or expression of *Dronc* were accompanied by an increased number of apoptotic *esg*$^{+}$ cells assayed by TUNEL method (Figure 2L) and anti-activated caspase-3 labelling (Figure S2F). These observations support the notion that homeostatic ISCs often overproduce in relation to demand and that a significant number of EBs is eliminated by apoptosis in low demand.

We hypothesized that when ECs are more rapidly renewed in the intestine the occurrence of EB death diminishes as the risk of EB accumulation is also lower. This would suggest that PCD in the adult midgut EBs is a tuneable process. Because all EBs express and require *Diap1* (Figure 1 and 2), we first hypothesised that cell death might be a 'default' fate of EBs that is counteracted by Diap1. We thus investigated how the EB death and life decisions might be regulated.

Enteroblast Death/Life Decision is Governed by Opposing Notch and EGFR Activity

PCD is essential during development, the removal of faulty cells during adult tissue homeostasis, the establishment of immune self-tolerance, and the killing by immune effector cells (Baehrecke, 2002; Mollereau et al., 2012; Protzer et al., 2008). Moreover, spontaneous apoptosis has also been observed in some adult tissues within the stem/precursor cell compartment (Domen and Weissman, 1999; Fuchs et al., 2013; Potten, 1992). Caspase-induced cell death in old or damaged cells often makes use of the cell death- and stress-responsive Jun N-terminal Kinase (JNK) cascade and it is typically associated with a compensatory proliferation to stimulate cell replacement (Biteau et al., 2008; Chen, 2012). In contrast, the purpose of culling excess but healthy cells is reducing their number and this type of apoptosis typically occurs without compensatory proliferation during development (Raff, 1996). We did not find evidence that apoptosis in the EBs may be regulated by JNK because EBs labelled by *Diap1-GFP* did not overlap with JNK activity measured using the JNK activity-sensitive reporter TRE-dsRED (Chatterjee and Bohmann, 2012) (Figure S3A and B). Thus, EB death appeared to be triggered by signals different to those regulating death of damaged or aged intestinal cells supporting the idea of a physiological cell death aimed at culling EB number.

The N and EGFR pathways are prime candidates as they often act antagonistically to promote cell death/life decisions during development (Dominguez et al., 1998; Protzer et al., 2008). Both N (Micchelli and Perrimon, 2006; Ohlstein and Spradling, 2007; Perdigoto et al., 2011) and EGFR (Biteau and Jasper, 2011; Jiang et al., 2011; Zhai et al., 2015) have critical roles in stem-cell renewal, EB specification, differentiation, and lineage commitment in adult gut homeostasis and regeneration (Biteau and Jasper, 2011; Jiang and Edgar, 2012; Kapuria et al., 2012; Perdigoto et al., 2011) but their role in EB death/survival has not been explored. We investigated the effect of cell-autonomous manipulations of N and EGFR signalling in EBs using the klu^{ReDDM} (Figure 3A-E). Changes in EB number were determined by quantification klu^{+} cells using lineage-tracing ReDDM (Figure 3F), complemented by assessment of

cell deaths within the progenitor cell compartment detected by GFP$^+$ TUNEL$^+$ cells using *esg*^{ReDDM} (Figure 3G). EC renewal (quantified as RFP$^+$-only cells) and non-autonomous effects on stem cells mitosis (PH3$^+$ cells) were also assessed in the *klu*^{ReDDM} guts with altered N and EGFR activity (Figure S3C and D).

EB-selective overexpression of the dominant negative form of N (Figure 3B) and of a constitutively active allele of EGFR protein (Figure 3C) both led to EB cells accumulation (compared to control Figure 3A). Endogenous over-activated N signalling by RNAi silencing of *Hairless* (*H)* (Figure 3D), the main antagonist of N (Bray, 2016), or by expression of a constitutively active N intracellular domain (data not shown) and expression of a dominant negative form of EGFR (Figure 3E) decreased EB number as assessed by reduced number of *klu*$^+$ cells (Figure 3F). Consistently, the loss of EBs caused by gain of N signalling or by *EGFR* inactivation in EBs was rescued by concomitant inhibition of apoptosis via *Debcl-RNAi* expression, also allowing new ECs to be formed (Figure 3H and I). Previous work has established that activation of EGFR in ISCs by EGF-like ligands produced by different intestinal cells in response to damage acts as a paracrine non-autonomous signalling, stimulating ISC proliferation (Biteau and Jasper, 2011; Jiang and Edgar, 2009; Zhai et al., 2015). In agreement with this, we observed that activation of EGFR in EBs using *klu*^{ReDDM} system, non-autonomously stimulated ISCs division (Figure 3, arrowheads indicate PH3$^+$, quantified in Figure S3 and extra ISCs labelled by Dl marker is shown in Figure 3C inset). These observations indicated that the massive accumulation of *klu*$^+$ EB cells in the midgut with constitutive activation of the EGFR pathway arose by both the suppressed EB deaths (autonomous effect) and increased ISC divisions (non-autonomous effect). Thus, in addition to its documented role in EB for stimulating ISC proliferation (Biteau and Jasper, 2011; Jiang and Edgar, 2009; Zhai et al., 2015), our data illustrate that the activity of EGFR is also crucial to suppress PCD in EBs. Consistently, we found that gain and loss of N and EGFR were accompanied by increased or reduced apoptotic *esg*$^+$ *GFP*$^+$ as assessed by TUNEL$^+$ method (Figure 3G), and that these gains and loses can be attributed to EB death/survival as shown in Figure 2). Specific manipulation in progenitors using *klu*^{ReDDM} also suggests that the increase in ISC division is likely a secondary consequence of progenitors escaping cell death (quantification of PH3$^+$ in Figure S3D).

Dl is the only N ligand acting in adult intestinal homeostasis and regeneration (Ohlstein and Spradling, 2007). Only ISCs express *Dl*, suppressing stemness in the neighbour daughter cell, driving N-mediated progenitor cell commitment towards the EC lineage (e.g. Ohlstein and Spradling, 2007; 2006; Perdigoto

et al., 2011). Our data suggests that Dl-mediated activation of N also 'primed' progenitor cells to PCD. Thus N and EGFR signalling counterbalances EB death/life decision in the adult midgut along with their crucial role in stem cell self-renewal, proliferation, differentiation, and lineage commitment e.g. (Jiang et al., 2011; Jiang and Edgar, 2009; Ohlstein and Spradling, 2007; Perdigoto et al., 2011; Zhai et al., 2015). This suggests that within the same cell, N and EGFR influence several cellular fates, including cell death. We hypothesize that EBs not receiving sufficient survival signals (e.g. $EGFR^{low}$) will be driven to PCD via the pro-apoptotic input by Dl-N signalling, while EBs with low N activation or receiving high anti-apoptotic input ($EGFR^{high}$) will accumulate undifferentiated or terminally differentiate upon receiving terminal differentiation input. These findings support that *Diap1* gene is a nodel point of the impact of N and EGFR activity in EB death/survival decision (see below and Discussion). In addition, N and EGFR signalling are both capable to promote terminal differentiation, suggesting that death/survival/differentiation may represent a continuum rathen than discreet cell fates.

Lozenge and Klumpfuss Pro-Apoptotic Factors Regulate the Undifferentiated Cell Culling, Fate Diversification, and Differentiation

To identify candidate transcription factors that may determine the outcome of N signalling, we focused on evolutionarily conserved N targets, the RUNX homologue Lozenge (Lz/RUNX) and Klu/WT1 (Protzer et al., 2008). Klu/WT is also a conserved mediator of PCD during development (Rusconi et al., 2004). Using antibodies against lz/RUNX protein and *lz-Gal4* reporter revealed that the occurrence of Lz^+ cells in a physiological midgut was extremely low (only 1-2 Lz^+ *per* posterior midgut; Figure S3E). Tracing the fate of lz^+ cells using lz^{ReDDM} showed that they are likely EB 'committed' to die as they did not yield differentiated ECs (Figure S3F). Consistent with this idea, blocking apoptosis via *p35* expression ($lz^{ReDDM}>p35$: Figure S3G) increased the number of cells derived from lz^+ progenitor, supporting that *lz*-expression may mark EB terminally fated to die. Forcing expression of *lz* in ISCs and EBs using esg^{ReDDM} led to significant increase in apoptotic esg^+ cells comparable to those obtained by manipulation of N and EGFR ($TUNEL^+$ esg^+, Figure 3G). Additionally, $esg^{ReDDM}>lz$ midgut also showed precocious terminal differentiation, reflected as small sized ECs (Figure S3H and H'), suggesting that Lz/RUNX is downstream of N signalling as no enteroendocrine ($Pros^+$) cells appear to be traced after *lz* overexpression. When *lz* was depleted via RNAi using klu^{ReDDM} during 7 days (Figure 3K), we observed a significant increase in EB number and, when using *esg-Gal4,* decreased $TUNEL^+$ esg^+ cells (Figure 3G). Quantification of EC turnover showed that EB loss was not due to terminal differentiation (Figure S3C)

and PH3^{+} labelling revealed that *lz*-RNAi in EBs also non-autonomously moderately increased ISC mitosis (Figure S3D). This observation is consistent with prior work in the developing fly retina (Behan et al., 2002; Siddall et al., 2003; Wildonger, 2005) showing that Lz promotes apoptosis through downregulation of EGFR signalling. Consistently, *lz* overexpression in ISCs/EBs using *esg*^{ReDDM} suppressed accumulation of EB caused by activated EGFR signalling (Figure S3I) while depleted *lz* partially suppressed EB loss by EGFR^{DN} (Figure S3J). Collectively, these findings suggest Lz is required for the irreversible commitment to death downstream of N, and possibly other factors yet to be defined in the adult *Drosphila* midgut. In EBs with sufficient survival signals, ectopic *lz* expression triggered precocious terminal differentiation. This supports that N-Lz axis also regulate terminal differentiation along with EGFR and other differentiationg signalling.

Overexpression and depletion of *klu* also influenced *esg*$^{+}$ cell death decision as detected by TUNEL method (Figure 3G). Additionally, a role of Klu in sustaining EC fate commitment was also uncovered from *klu-RNAi* experiments using *esg*^{ReDDM} and *klu*^{ReDDM} (see Figure S3). EC fate determination requires the Dl-mediated activation of N signalling in EBs (Kapuria et al., 2012; Perdigoto et al., 2011). In the absence of N activation, upon stem cell division both daughter cells adopt the ISC fate or terminally differentiate as EEs, which can be marked by Pros (Jiang and Edgar, 2012). However, in the presence of a high Dl-N signalling, the daughter cell receiving N signalling commits to differentiation towards the EC lineage, which is reflected by the committed progenitor cell increasing its size over time via endoreplication (Lucchetta and Ohlstein, 2012; Perdigoto et al., 2011). This fate-determination is generally depicted as an irreversible commitment. However, we observed that depleting *klu* by RNAi in EBs (using *klu*^{ReDDM}) which is normal gut will only yield ECs caused a switch of their fate towards the EE lineage (Figure S3K-N). *klu* RNAi midguts showed cells with large nuclei (high DNA content shown by DAPI indicate polyploid cells) labelled with Pros (red arrowheads, Figure S3K), supporting conversion of EC-'committed' EBs towards the EE lineage. Typically wild type midguts have a ratio of 10% EE (Pros^{+}) and 90% EC (de Navascués et al., 2012), and no EE cells are normally derived by *klu*$^{+}$ progenitors (Figure S3M). However, *klu* depleted *klu*$^{+}$ EBs (*klu*^{ReDDM}>*klu-RNAi*, 7 days) generated approximately 33% of EEs instead of 0%, indicating a continuous requirement for *Klu* gene expression to maintain the EC commitment fate. This experiment also uncovered an unanticipated plasticity of EBs to adopt an alternative fate. These experiments can be interpreted in two alternative models. In one model, Klu^{+} activity is required in all EBs for their robust establishment of the EC lineage, as well the regulation

of their number. In the second model, ISCs generates stochastic EC and EE cell fates (~50% EC and ~50% EE) but N activation, and upstream signals such as insulin, could bias the fate towards EC lineage, resulting in ~00% EC and ~10% EE. In such scenario, Klu^{+} would be required to robustly maintain the EC fate in a subset of the EBs, which could account for the observation that EC fate still occur in klu^{ReDDM}>*klu-RNAi* guts. Regardless the mechanism, these findings are in line with recent studies of mammalian stem cell systems that suggest that progenitor cells are primed, not committed, and cell fate decisions remain tuneable by external inputs (Notta et al., 2015).

Comparison of Models with a Feedback Mitosis Control and a 'Tuneable' Apoptosis with Steady Stem Cell Divisions

Both PCD and stem cell division are energetically costly (Vaux and Korsmeyer, 1999). Thus, to further explore the potential advantages of this apparently costly strategy for adult tissue renewal, we built a computational model based on these experimental observations to evaluate the performance of a stem cell system in response to injury. We compared a hypothetical system controlling production only by mitosis with a system in which stem cells produce a continuous pool of progenitor cells with further control of their numbers by PCD. The model includes a feedback mechanism by which the steady-state number of EC determines both the rate of ISC division and the probability of EB to undergo either differentiation or apoptosis (Figure S4). The model predicts a tighter control of the number of EC under homeostatic conditions and a faster recovery from acute damage (a sudden EC loss for example through injury) (Figure 4A and B).

A simulated intestinal turnover with single (Figure 4A) and two successive challenges (Figure 4B) revealed that both models cope with a loss of around 30 EC per day, which was the observed average intestinal cell loss in 'Low demand' ReDDM-tracing experiment (Figure 1A, right graph). However, when we challenged the models with one or two successive acute damages (Figure 4A and B, respectively), only the model with pre-existing EBs owing to continual ISC divisions predicted returns to homeostasis after one to two days consistently with the estimated recovery time determined by previous experimental studies (Amcheslavsky et al., 2008; Buchon et al., 2009; Jiang and Edgar, 2011).

These simulations hinted at EB death fate in the intestine being a tuneable fate decision presumably by extrinsic cues that also stimulate EB differentiation for cell replacement. Consistent with this idea, we noticed that EB express a varying level of *Diap1* (assessed by GFP fluorescent intensity, Figure 4C).

Importantly, single manipulations of EGFR, N activity or caspases inhibition markedly changed numbers of *Diap1*$^{+}$ cells (EBs: Figure 4D; see also quantification of terminal differentiation, new ECs in Figure 4E) along with Diap1 levels as assessed by changes in their fluorescent intensity (Figure 4C). The baculovirus *p35* antiapoptotic factor blocks apoptosis downstream of the *Diap1* transcriptional repression by Rpr/Hid/Grim factors (Bergmann and Steller, 2009; Hirata et al., 1995; Holley et al., 2002; Meier et al., 2000). As anticipated, expression of the *p35* caused accumulation of EBs with many of them exhibiting low Diap1-GFP levels (Figure 4C and D). This would suggest that EBs cells displaying low Diap1 levels would normally undergo PCD but escape death by expressing the anti-apoptotic factor *p35*. Importantly, this 'tuneable' *Diap1*-GFP is also observed when gene manipulations are done using another promoter, *esg-Gal4* (Figure 4F). Note that EBs with constitutively active EGFR had an excess of EBs but with highly variable Diap1-GFP fluorescence level intensity (Figure 4F) as seen in quantification in Figure 4C with the *klu-Gal4*, supporting that *Diap1* transcription is tuneable by various signals simultaneously. This is consistent with *Diap1* transcription being directly regulated by several pathways (Zhang et al., 2008), most notably including the Dl-N pathway itself (Djiane et al., 2013) (see also Discussion).

These observations indicate that adult ISC overproduce progenitor cells (EBs) and compensate this 'overproduction' by a culling excess supply via a caspase-dependent death programme through a N-Klu-Lz cascade analogous to the PCD that eliminate excess cells during retinal development e.g. (Begmann and Steller, 2009; Baker et al. 2001). Early findings of spontaneous apoptosis in the human and murine intestinal stem/progenitor cell compartment (Potten et al., 2002) were attributed to a protection strategy to eliminate damaged or aged stem cells. Recently studies in mice have shown that endogenous apoptosis helps to regulate stem or progenitor cell numbers and regeneration (Fuchs et al., 2013). Our study thus provides a paradigm for how the culling process may operate during cell turnover and how this process is interwoven with proliferation and cell fate determination to ensure that the correct cell types and number are produced.

DISCUSSION

We have found that steady-state intestinal stem cells production is not solely controlled by mitosis, but also by a culling process of progenitors. Our observations support a model whereby adult ISC overproduce progenitor cells to ensure rapid intestinal cell renewal in the face of sudden and

unpredictable demands, thereby efficiently preserving homeostasis and intestinal barrier. Under normal physiological conditions, demand equals supply by ISCs, but in low demand (e.g. during period of fasting) the ISC's production exceeds the tissue demand and EB number is adjusted by a N-Klu-Lz-mediated death via caspase-dependent programme. We have also shown that the elimination of surplus EBs is a critical tumour suppressor strategy. Thus ISCs performance both promote and limit tumorigenesis, and this findings may explain earlier observations of regeneration defects when endogenous inhibitors of apoptosis were impaired (Fuchs et al., 2013). Moreover, our study identifies nodal points for N and EGFR. including Diap1 (survival) and an effector of cell death Lz. Our epistatic data suggest that Lz may mediate cross-talk between N and EGFR to reinforce cell death commitment by dampening EGFR signalling downstream of the receptor as seen during development (Wildonger, 2005), which may explain how these pathways determine robust outcomes of N signalling.

N signalling requires the continuous interaction of N protein with its membrane-bound ligand Dl in the adjacent stem cells (Ohlstein and Sprandling, 2007; Simon and Clevers; 2011, Liang et al., 2017). EGFR signalling can be activated in the EB in response to multiple EGF-like signals released by the niche, as well as dying ECs (Liang et al., 2017) that also stimulate ISC's proliferation, providing different scenarios for how survival signals may modulate committed progenitor-cell numbers. N and EGFR oppositely control death and life decisions in other cellular context during development (Baker and Yu, 2001; Gilboa and Lehmann, 2006; Protzer et al., 2008). However, in these other developmental contexts apoptosis is highly stereotyped with an invariant outcome and often occurs after cell fate determination. In adult tissues with high and constant demand for cell turnover, the supply of precursor cells needs to be regulated dynamically and adaptively in coordination with cell fate diversification to respond efficiently to changing environmental conditions and with sudden increase in demand. Indeed, while N and EGFR act oppositely to control death/survival of EBs, they are both positively required for EB terminal differentiation. Moreover, the fact that Dl-N signaling can directly drive expression of both *rpr* (Krejci et al., 2009) and *Diap1* (Djiane et al. 2013) supports that N activation may 'prime' EB to death and that execution of the death programme depends on the balance of pro-apoptotic and pro-survival signals the EB cells receive, which may be reflected by *Diap1* levels. These data also indicate that EBs are actually executing ternary (self-renewal, death, or differentiation) not binary choice (self-renewal or differentiation).

We postulate that a death signal emanating from the stem cells in direct contact with its committed

progeny allows a flexible accommodation of EB-number to ISC production. This death programme is also tuneable by survival signals produced by dying differentiated cells, from the niche, or other environmental cues, which further attunes EB-number regulation to varying physiological and pathological conditions. In the haematopoietic system stochastic cell choice provides flexibility for the maintenance of production of all blood cell lineages in the face of substantial demand for one particular lineage (Enver et al., 1998). In a speculative manner, we suggest that ISC dividing ahead of demand may similarly generate stochastic cell choice (EC and EE) with a high N-Klu biased fate towards the EC lineage. Derangement of apoptosis-mediated EB number regulation along with fate conversion may explain the previously observed tumors associated with impaired N signalling (Biteau et a., 2011) as supported by our findings (Figure 1J). Similarly, the same mechanism of altered apoptosis within the stem/progenitor cell compartment causes hyperplasia and tumour formation in the murine intestine (Fuchs et al., 2013). Our study provides a regulatory logic for the adjustment of progenitor numbers intertwined with both fate diversification and tissue demand.

EXPERIMENTAL PROCEDURES

Drosophila **Stocks and Husbandry**

The following alleles and fly stocks, as described in FlyBase (http://flybase.org/), were used (source in STAR methods)

For ReDDM tracing (*UAS-mCD8::GFP*, *UAS-H2B::RFP*, *Tubα1-Gal80^{ts}*; as described in ref. (Antonello et al., 2015), the following Gal4 drivers were used: *esg-Gal4* (J. Casanova), *klu-Gal4* (T. Klein), *GBE-Su(H)-Gal4* (S. Bray), *lz-Gal4* (FBtp0099102).

Reporter transgenes: Notch activity-sensitive sensor, *GBE-Su(H)-m8-lacZ* and *NRE-GFP* [S. Bray; (Housden et al., 2012)]; the caspase activity sensor *UAS-Apoliner* [J. P. Vincent; (Bardet et al., 2008)], *Diap1-GFP.4.3* (Zhang et al., 2008), JNK activity-sensor *TRE-dsRED* (M. Chatterjee and Ip, 2009) (FlyBase ID: FBal0268835).

Other mutant allele and fly stocks used were: UAS-p35x2 (two insertions, B. Hay), *hsp70-Gal4* (FlyBase ID: FBst0002077), *UAS-Debcl-RNAi* (TRiP.JF02429), *UAS-Dredd-RNAi* (TRiP.HMS00063), *UAS-*

Drice-RNAi (TRiP.HMS00398), *UAS-Dark-RNAi* (TRiP.HMS00870), *UAS-Dronc.S* (BDSC:56197, FlyBase ID: FBst0056197), *UAS-Diap1-RNAi* (TRiP.HMS00752), *UAS-klu-RNAi* (TRiP.JF03158), *UAS-N^{DN}* (J. Treisman), *UAS-N^{ICD}* (Flybase ID: FBal0093233), *UAS-$EGFR^{DN}$* (FlyBase ID: FBtp0007539), *UAS-$EGFR^{act}$ (EGFR::tor^{act}* (Dominguez et al., 1998)), *UAS-H-RNAi* (KK104341), *UAS-lz* (FlyBase ID: FBtp0125780), *UAS-lz-RNAi* (TRiP. JF02221), *UAS-klu* (T. Klein), *Df(3L)H99* (FlyBase ID: FBst0001576), *w^{1118}* (FlyBase ID: FBst0003605).

Fly crosses were performed at 18 ºC and reared on standard 'Iberian' food. Standard 'Iberian' fly food was made by mixing 15 L of water, 0.75 kg of wheat flour, 1 kg of brown sugar, 0.5 kg yeast, 0.17 kg agar, 130 mL of a 5% nipagin solution in ethanol, and 130 mL of propionic acid. Upon eclosion, adult female flies of 3-4 days old from control and experimental genotypes were shifted to 29 °C in the presence of males and transferred to new food vial every 2 days ('Low' demand condition) or every 7 days ('Variable' demand under standard culturing conditions).

Immunostaining

Adult *Drosophila* midguts were dissected, fixed for 40 min in 4% PFA, and stained using the following primary antibodies in PBT buffer (PBS, 0.1% Triton X100): rabbit anti-activated caspase3 (1:2000, Upstate), rabbit anti-PH3 (1:2000, Upstate), mouse anti-Dlg-1 (1:100, Hybridoma Bank), mouse anti-Pros (1:100, Hybridoma Bank), mouse anti-Dl (1:100, Hybridoma Bank), mouse anti-lz (1:100, Hybridoma Bank), sheep anti-GFP (1:1000, Biogenesis), chicken anti-β-Gal (1:1000, Abcam) and the according Alexa secondary fluorophore coupled antibodies (1:500, Invitrogen). Nuclei were counterstained with DAPI (Sigma) and mounted in Fluoromount-G (Southern Biotech).

TUNEL Assay in Stem and Progenitor Cells

Adult midgut of the indicated genotypes and age were dissected, fixed, and immunostained to detect dying GFP-labelled progenitor cells by in situ Cell Death Detection Kit (Roche Applied Science, Grenzach, Germany) according to manufacturer´s protocol followed by a DAB-reaction (Thermo Fisher, Schwerte, Germany). GFP^+ve and $TUNEL^+$ve cells were quantified using a Nikon Fluorescence microscope (Eclipse 90i). Data represent the proportion of $TUNEL^+$ve cells relative to total GFP^+ve cells. Graphs and all statistical analyses were performed using Graphpad Prisma 6, and data were analysed using ANOVA analysis of variance with Bonferroni correction statistical test and Student´s t-tests.

Image Acquisition

Confocal images were obtained with a Leica TCS SP5 inverted confocal microscope, using a 1024 × 1024 image size. Stacks were typically collected every 1 µm and the images were reconstructed using max projection. Images were evaluated and scaled using Fiji/ImageJ. In all cases, the images shown in the Figures are representative of the effect of the genetic manipulation.

Quantitative PCR

To assess the efficacy of the RNAi transgenes, mRNA was extracted from wandering third instar larvae with the corresponding RNAi transgene (*hsp70-Gal4 > UAS-RNAi*) or without (control, *hsp70-Gal4 >*) after a 1 h heat shock at 37 °C to induce transgene expression. To determine mRNA levels we used superScript First-Strand Synthesis System for RT–PCR (Invitrogen) and SYBR Green PCR Master kit (Applied Biosystems), according to the manufacturer's instructions. The cDNAs were amplified using specific primers designed using the ProbeFinder software by Roche Applied Science, and *RpL32* was used as a house-keeping gene for normalization.

The following primers were used:

Gene	Forward	Reverse
Drice	TGTCGGCCCACCCTTATCTA	TGGACGACCATGACACACAG
Debcl	ATCATCAACCAGGGGAAATGTCTG	GTTGCGCAAACGCTGTGTC
H	AACTGTGACCCCAACGTCG	CGAGCTGTTGTCGTCCGAA
lz	TTCACCAGGATCTATTGTGGATGG	ATTGCTCGTGCGCACCAATTC
klu	ACCGTCTAAATCAAAGAGTCCCA	TGGCCACAAGATATCCAGCC
N	ACCGTTCGCGGAACTGATACC	GCGCAGTAGGTTTTGCCATTG
RpL32	TGTCCTTCCAGCTTCAAGATGACCATC	CTTGGGCTTGCGCCATTTGTG

Quantification and Statistical Analysis, Cell Counting and Fluorescence Measurements

For progenitor cell counts, 20x images of ReDDM midguts of the different genotypes and conditions were cropped with ImageJ (Fiji 64bit) for processing and quantification with Matlab. A self-written script optimized for the ReDDM method that analyses quality (size, colour) and quantity (count events) in posterior midguts was used to measure the number of progenitor cells (double positive mCD8::GFP H2B::RFP cells) and DAPI nuclei (Antonello et al., 2015). Measurements of fluorescence intensity of

Diap1-GFP levels were acquired with a fixed 488nm laser intensity and images of the Diap1-GFP midguts were analysed using a Fiji-script for intensity per cell available from the authors. Representative images are shown in all panels. For initial experiments exploring the role of apoptosis, at least 20 posterior midguts were scored. For complex experiments analysing many genes conditions usually cell counting were done in at least four to 10 posterior midguts.

Mathematical model and equations are described in **Supplementary Information**

ACKNOWLEDGMENTS

We thank T. Klein, P. Adler, K. Dücker and J-P. Vincent for fly stocks; the Bloomington *Drosophila* Stock Center (NIHP400D018537), the Transgenic RNAi Project (TRiP) at Harvard Medical School (NIK/NIGMS R01-GM084947), and the Vienna Drosophila Resource Center (VDRC, http://www.vdrc.at) for providing transgenic RNAi fly stocks. We also thank I. Oliveira and L. Mira for technical assistance. T.R. was funded by a postdoctoral Deutsche Forschungsgesellschaft (DFG) fellowship and by a contract by Foundation Botin, and Z.A.A. by a fellowship from MEC-CONSOLIDER. This work was funded by a Generalitat Valenciana Grant (PROMETEO/2017/146), Foundation Botin, Fundación Científica AECC (AECC CICPF16001DOMÍ) and the Ministry of Economy and Competitiveness Grants (SEV-2013-0317 and MICCIN BFU2015-64239-R) to M.D.

Author contributions: T. R., Z.A.A., and E.B. performed the experiments and analyses and contributed to the design of the study. S.P. M.N. and L. M-O developed the computational models. M.D. provided the general concept, the study design, interpretation, and supervision and T.R., Z.A.A., and M.D. wrote the paper.

The authors declare no Competing Interests.

Correspondence and requests for materials should be addressed to M.D. (e-mail: m.dominguez@umh.es).

FIGURE LEGENDS

Figure 1. Inhibition of Bpoptosis in ISCs and Enteroblasts and Endogenous Expression of Diap1 in Enteroblasts.

(A) Scheme for tracing intestinal progenitor cell number regulation in midgut with low intestinal renewal ('Low') using the lineage tracing ReDDM system (Antonello et al., 2015). The strategy relies on minimizing exposure of flies to contaminated food by transferring flies to fresh food vials every two days ('Low') as compared with normal culturing conditions in which flies are typically transferred to fresh food vial every week. This 'Low' demand strategy effectively minimized intestinal renewal. (B) Scheme of the ReDDM tracing method. This system uses two fluorescent transgenes with short- (membrane CD8::GFP, green) and long-term (nuclear H2B::RFP, red) stability and the Gal80 repressor (*tubα1-Gal80^{ts}*) for temporal control of UAS-driven transgenes. Using *esg-Gal4*, the reporter transgenes are seen in the ISCs and EBs (detected as double labelled cells). Newly renewed ECs or EEs are traced by the nuclear RFP owing to the protein stability of H2B::RFP (Antonello et al., 2015). (C) Quantification of renewed ECs (red-only labelled cells) in posterior midguts after 7, 14, or 21 days of tracing in normal ('Variable': gut scored n= 9, 8, 4) and low demand ('Low': n= 6, 4, 7) culturing conditions. Error bars are Standard Error of the Mean (SEM) and asterisks denote significances from one-way ANOVA with Bonferroni's Multiple Comparison Test (**** = $p < 0.0001$). (D) Quantification of mitosis (phospho-histone H3 (PH3)$^{+}$*-ve* cells) in low demand midguts at the indicated time points. *n.s.* not significant from one-way ANOVA test. (E) Representative adult midgut from control *esg^{ReDDM}* at day 7 after temperature shift in variable demand (normal culturing condition). ECs renewed are marked positively by persistent RFP labelling (red-only cells). (F and G) Few ECs had been renewed in 'Low' midguts after 14 (F) and 21 (G) days of tracing. (H-J) Age-synchronized posterior midguts of control (*esg^{ReDDM}>*, H) and *p35* overexpression in stem and progenitor cells (*esg^{ReDDM}>p35*, I and J) at 7 days after temperature shift . Arrow in J points to an undifferentiated tumour mass in *esg^{ReDDM} >p35* anterior midgut. (K-M) *Diap1* is detected in adult midgut in EBs. *Diap1* is monitored by the *GFP.4.3.* (green) reporter that faithfully reflects endogenous expression (Djiane et al., 2013; Zhang et al., 2008). Diap1-GFP^{+}*ve* cells co-localized with EB marker *GBE-Su(H)-lacZ* (Figure 1F-G) and were negative for mitotic marker PH3 (red, inset in K). (L and M) *Diap1-GFP* is negative for differentiated cells, e.g. EE marker Prospero (Pros, grey in M). ISCs and EBs and their differentiated progeny were traced by RFP (*esg^{ts}>H2B::RFP*). Guts are counterstained with DAPI (blue).

Figure 2. Physiological Caspase-Dependent Apoptosis of Enteroblast Cells in the Adult Midgut

(A) Schematic representation of the apoptotic pathway in *Drosophila.* (B and C) Images of guts of adult age-synchronized female flies carrying the *Diap1-GFP* reporter in control (B) and heterozygote for *Df(3L)H99,* a chromosomal deficiency for the pro-apoptotic gene *rpr, hid, grim* (C). (D) Measurement of Diap1-GFP^{+} cells in posterior midguts of the indicated genotypes 7 days after temperature shift in "Low" culturing condition (p < 0,03, Student´s t-test, n=6 and 7 respectively). (E-I) Adult *klu*^{ReDDM} midguts (7 days after temperature shift) showing EBs (double labelled green red cells) and newly differentiated ECs (red-only cells) in control (F) or expressing RNAi transgenic lines against *Debcl* (G), *Drice* (H) or *Diap1* (I). (J) Quantification of *klu*$^{+}$ cells in the indicated midguts at day 7 in low demand (Low) or standard (Variable) culturing conditions (n=7, 5, 9, 7). (K) Intestinal cell turnover measured by quantification of the number of newly renewed ECs (red-only cells: gut scored n=9, 13, 9, 13). (L) Quantification of apoptotic progenitor cells (*esg*$^{+}$) measured as GFP^{+} TUNEL^{+} (n= 9, 9, 9, 9). Box and whisker plot showing the means and values range. P values (p < 0,02) calculated by one-way ANOVA with Bonferroni correction. Scale bars, 100µm.

Figure 3 Enteroblast Death/Life Decision is Governed by Opposing Notch and EGFR Activity

(A-E) and (H-M) Confocal images of representative midguts of the indicated genotypes using *klu*^{ReDDM} for tracing and age-and EB-specific transgene expression at day 7 after temperature shift. ISCs mitosis was monitored by using PH3 labelling (white) in all guts. Accumulation of EBs in midguts with constitutively activated EGFR (*klu*^{ReDDM}> *EGFR*^{act} is accompanied with non-autonomously increase in ISC mitosis. Inset shows labelling with Dl (blue) shown in C, revealing symmetric ISC mitoses as previously shown (Jiang and Edgar, 2009). (F) Quantification of the number of *klu*$^{+}$ (EBs) in the indicated midguts (n= 21, 14, 5, 6, 8, 6, 4, 10, 12, 9, 13, 14). (G) Quantification of apoptotic *esg*$^{+}$ TUNEL+ cells in the indicated midguts (n= 28, 4, 7, 7, 16, 8, 8, 7, 10, 7, 20, 24). **, p< 0.01; ****, p< 0.0001, one-way ANOVA with Bonferroni correction. Quantification of EC renewals is in Figure S3. (H and I) Rescue of the loss of EBs induced by gain of Notch (*H-RNAi*) or the loss of EGFR (*EGFR*^{DN}) by expressing *Debcl-RNAi*. (J and K) Impact of loss by RNAi expression (J) and gain (K) of *lz* using *klu*^{ReDDM} (see Figure S3C, D and H for quantification and Extended Data). (L and M) Impact of loss by RNAi expression (L) and gain (M) of *klu* using *klu*^{ReDDM}. White arrowheads point to examples of mitosis labelled by PH3^{+}. Scale bars, 100µm.

Figure 4. Tunable Apoptosis Through Tunable Diap1 Signals

(A and B) Number of EC over time (left), number of EB over time (middle), and probabilities of EB lost through apoptosis (right graph). (C) All EBs show Diap1-GFP expression but at varying levels, consistent with EB death fate being tuned by apoptotic input counteracting survival signals. (D) Quantification of the number of Diap1-GFP^{+}. Notet that in p35-expressing midguts reared in LD GFP levels are not increased, consistent with p35 protein suppressing apoptosis downstream of Diap1. (E) Quantification of the number of newly renewed EC in the indicated genotypes after 7 days (n= 17, 13, 12, 10, 21, 24). Increase in EB numbers and EC turnover in EGFR^{act} midgut reflects both suppression of EB deaths and the non-autonomous stimulation of ISC in this background. P values were calculated using one-way ANOVA Bonferroni corrected (**** $p < 0{,}0001$). (F) Representative images acquired using the same laser intensity are shown for Diap1-GFP in the indicated illustrative examples.

SUPPLEMENTAL FIGURE LEGENDS

(Figure S1 Related to Figure 1)

Figure S1. Evidence of Apoptotic Enteroblasts and Novel Enteroblasts Markers

(A-C) Apoliner caspase sensor construct is driven by *esg*-Gal4. The caspase sensor codes for a membrane targeted fusion protein of mRFP and eGFP that upon cleavage through the caspases Drice and Dcp-1 unmasks a NLS and translocates eGFP into the nucleus (Bardet et al., 2008). Representative image of adult homeostatic posterior midgut carrying the caspase activity reporter *UAS-Apoliner* driven in ISCs and EBs by *esg-Gal4* are shown. Nuclear staining (green) denotes Caspase 3 activity. Arrows point to examples of EBs with caspase activity (magnification in B). Midguts were counterstained by DAPI (blue, C). (D-D") *Diap1*$^{+}$ (green) cells are positive for the EB marker *GBE-Su(H)-lacZ*, a reporter of Notch activity, and negative for the ISC marker Delta (Dl, grey). (E and F) The Gal4 enhancer trap in *klu* gene (hereafter *klu>*) drives expression in EBs as visualized by co-localization of *UAS-RFP* with two Notch activity reporters, *GBE-Su(H)-lacZ* (E-E") and (F) *NRE-GFP*. The expression levels of *klu* and Notch reporters are variable within individual EB cells. (G and H) Lineage-tracing using ReDDM and *klu-Gal4*. The *klu*-derived cells are strictly of the EC lineage as visualized by the Dlg-1 marker (grey) and large nuclei (Red-only cells) and lack of EE marker Pros (data not shown). Scale bars, 100µm.

(Figure S2 Related to Figure 2)

Figure S2. Knockdown of Caspases Dark and Dredd and Overexpression of Caspase Dronc in Enteroblasts

(A-E) Representative confocal images of posterior midguts of control (A and D) and *Dark-RNAi* (B), *Dredd-RNAi* (C) and unprocessed *Dronc* (*UAS-Dronc.s*) overexpression at day 7 after temperature shift using *klu*^{ReDDM} system. Mitosis is monitored b PH3 staining (grey dots). (F) Histogram of quantification of the number of double GFP^{+}, cleaved caspase 3 $^{+}$ cells per posterior midgut in the indicated genotypes. *** $P< 0.001$, one-way ANOVA analysis of variance with Bonferroni correction. Control guts *klu*^{ReDDM}> (n=17), *klu*^{ReDDM}>*Dronc*.s (n=14), and *klu*^{ReDDM}>*Dark-RNAi* (n=12). Scale bars, 100µm. (G) Quantitative

RT-PCR assays of the efficacy of the indicated RNAi transgenes using *hsp70-Gal4* stimulation (one hour heat-shock at 37ºC).

(Figure S3 Related to Figure 3)

Figure S3. Lz and Klu Signals in the Apoptotic Control of Enteroblast Culling and Fate Diversification

(A and B) Representative homeostatic midgut labelled with the RFP sensor of JNK activity (red) and Diap1-GFP (green). JNK activity is not detected in progenitor cells. Note JNK^+ cells are matured ECs as visualized by the Dlg1 marker (grey). (C) Quantification of the number of RFP-only cells (new ECs, n= 18, 14, 7, 6, 6, 4, 10, 12, 9, 13, 14, 9, 9). Number of migut scored for the indicated genotypes are indicated. (D) Quantification of the number of ISC $PH3^+$ cells in posterior midguts with or without apoptosis in EBs (n= 15, 9, 14, 5, 4, 6, 14, 12, 9, 13, 14). ** P<0.01; ***P<0,001; ****P<0.0001, one-way ANOVA with Bonferroni correction. (E) Adult homeostatic midgut staining with anti-Lz antibody (pink nuclei, arrowheads). (F and G) Midguts of control lz^{ReDDM} (F) and with *p35* overexpression (G). Note that Lz^+ progenitor cells generated differentiated progeny (red cells in **g**) only when apoptosis was blocked. (H-H') Overexpression of Lz in ISCs and EBs by esg^{ReDDM} caused precocious differentiation (red-only cells). Differentiated EC are labelled by the epithelial marker Dlg-1 (blue). Note the small size of the new EC denoting precocious terminal differentiation. (I) *lz* overexpression can suppress EB accumulation driven by $EGFR^{act}$. (J) *lz-RNAi* can partially rescue loss of ISC and EBS and mitotic defects caused by expression of $EGFR^{DN}$ in ISCs and EBs by *esg-Gal4*. (K-M) *klu-RNAi* in ISCs and EBs (K) and only EBs (L) and control klu>RFP gut (M). Red arrowhead in K point to large nuclei Pros+ RFP+ cells. Old EEs are negative for RFP. In wild-type midguts all or almost all Klu-derived cells take on the EC fate and are negative for EE marker Pros (green). (N) Quantification of percentage of EEs in guts of the indicated genotype 7 days after expression of transgene and tracing normalized against control (n= 7 and 10 respectively). All Images show midguts at day 7 after temperature shift. Scale bars, 100µm, excepts: D, 25µm. H and I, 25µm.

(Figure S4 Related to Figure 4)

Figure S4. Enterocyte fluctuations at steady state in the Model of Mitotic Control only (M) and Homeostatic Control Based on Continual Mitosis and Tunable Apoptosis (M-A).

(A) Fluctuating number of EC around a steady state value during a period of 30 days, in the Mitosis (M) model (dashed red line), and in the Mitosis-Apoptosis (M-A) model (solid red line). Histograms of the numbers of EC for the M model (middle) and for the M-A model (right). (B) Fluctuating probabilities of differentiation (pD , brown lines) or apoptosis (pA, black lines) for the enteroblasts, in the same time period, for the M model (dashed lines), and the M-A model (solid lines). (C) Fluctuations of the cycle time (in

hours) of the intestinal stem cells inferred from the M model (dashed line) and the data from M-A model (solid line). (D) Fluctuations in the life time of enteroblasts (in hours) in the M-A model.

REFERENCES

Amcheslavsky, A., Jiang, J., Ip, Y.T. (2008). Tissue Damage-Induced Intestinal Stem Cell Division in Drosophila. Stem Cell *4*, 49–61.

Antonello, Z.A., Reiff, T., Ballesta-Illan, E., Dominguez, M. (2015.)Robust intestinal homeostasis relies on cellular plasticity in enteroblasts mediated by miR-8-Escargot switch. The EMBO J. *34*, 2025–2041.

Apidianakis, Y., Rahme, L.G. (2010). Drosophila melanogaster as a model for human intestinal infection and pathology. Dis Models & Mech *4*, 21–30.

Baehrecke, E.H. (2002). How death shapes life during development. Nat Rev Mol Cell Biol *3*, 779–787.

Baker, N.E., Yu, S.Y. (2001). The Egf receptor defines domains of cell cycle progression and survival to regulate cell number in the developing Drosophila eye. Cell *104*, 699–708.

Bardet, P.L., Kolahgar, G., Mynett, A., Miguel-Aliaga, I., Briscoe, J., Meier, P., Vincent, J.P. (2008). A fluorescent reporter of caspase activity for live imaging. Proceedings of the National Academy of Sciences *105*, 13901–13905.

Behan, K.J., Nichols, C.D., Cheung, T.L., Farlow, A., Hogan, B.M., Batterham, P., Pollock, J.A. (2002). Yan regulates Lozenge during Drosophila eye development. Development Genes and Evolution 212, 267–276.

Bergmann, A.A., Steller, H.H. (2009). Apoptosis, stem cells, and tissue regeneration. Sci Signal *3*, re8–re8.

Biteau, B., Hochmuth, C.E., Jasper, H. (2011). Maintaining Tissue Homeostasis: Dynamic Control of Somatic Stem Cell Activity. Cell Stem Cell *9*, 402–411

Biteau, B., Hochmuth, C.E., Jasper, H. (2008). JNK Activity in Somatic Stem Cells Causes Loss of Tissue Homeostasis in the Aging Drosophila Gut. Stem Cell *3*, 14–14.

Biteau, B., Jasper, H. (2011). EGF signaling regulates the proliferation of intestinal stem cells in Drosophila. Development *138*, 1045–1055.

Bray, S.J. (2016). Notch signalling in context. Nature *17*, 722–735.

Buchon, N., Broderick, N.A., Poidevin, M., Pradervand, S., Lemaitre, B. (2009). Drosophila Intestinal Response to Bacterial Infection: Activation of Host Defense and Stem Cell Proliferation. Cell Host & Microbe *5*, 200–211.

Chatterjee, M., Ip, Y.T. (2009). Pathogenic stimulation of intestinal stem cell response in Drosophila. J. Cell. Physiol. *220*, 664–671.

Chatterjee, N., Bohmann, D. (2012). A Versatile ΦC31 Based Reporter System for Measuring AP-1 and Nrf2 Signaling in Drosophila and in Tissue Culture. PLoS One *7*, e34063.

Chen, F.(2012). JNK-induced apoptosis, compensatory growth, and cancer stem cells. Cancer Res *72*, 379–386.

de Navascués, J., Perdigoto, C.N., Bian, Y., Schneider, M.H., Bardin, A.J., Martinez Arias, A., Simons, B.D. (2012). Drosophila midgut homeostasis involves neutral competition between symmetrically dividing intestinal stem cells. The EMBO J. *31*, 2473–2485.

Djiane, A., Krejčí, A., Bernard, F., Fexova, S., Millen, K., Bray, S.J. (2013). Dissecting the mechanisms of Notch induced hyperplasia. The EMBO J.*32*, 60–71.

Domen, J.J., Weissman, I.L.I. (1999). Self-renewal, differentiation or death: regulation and manipulation of hematopoietic stem cell fate. Mol Med Today *5*, 201–208.

Dominguez, M., Wasserman, J.D., Freeman, M. (1998). Multiple functions of the EGF receptor in Drosophila eye development. Curr. Biol. *8*, 1039–1048.

Enver, T.T., Heyworth, C.M.C., Dexter, T.M.T. (1998). Do stem cells play dice? Blood *92*, 348–352.

Fuchs, E., Chen, T. (2013). A matter of life and death: self-renewal in stem cells. EMBO Rep *14*, 39–48.

Fuchs, Y., Brown, S., Gorenc, T., Rodriguez, J., Fuchs, E., Steller, H. (2013). Sept4/ARTS regulates stem cell apoptosis and skin regeneration. Science *341*, 286–289.

Fuchs, Y., Steller, H. (2011). Programmed cell death in animal development and disease. Cell *147*, 742–758.

Furriols, M., Bray, S. (2000). Dissecting the mechanisms of Suppressor of Hairless function. Dev. Biol. *227*, 520–532.

Gilboa, L., Lehmann, R. (2006). Soma-germline interactions coordinate homeostasis and growth in the Drosophila gonad. Nature *443*, 97–100.

Hirata, J., Nakagoshi, H., Nabeshima, Y., Matsuzaki, F. (1995). Asymmetric segregation of the homeodomain protein Prospero during Drosophila development. Nature *377*, 627–630.

Holley, C.L., Olson, M.R., Colón-Ramos, D.A., Kornbluth, S. (2002). Reaper eliminates IAP proteins through stimulated IAP degradation and generalized translational inhibition. Nat Cell Biol *4*, 439–444.

Housden, B.E., Millen, K., Bray, S.J. (2012). Drosophila Reporter Vectors Compatible with ΦC31 Integrase Transgenesis Techniques and Their Use to Generate New Notch Reporter Fly Lines. G3: Genes|Genomes|Genetics *2*, 79–82.

Jiang, H., Edgar, B.A. (2012). Intestinal stem cell function in Drosophila and mice. Current Opinion in Genetics & Development *22*, 354–360.

Jiang, H., Edgar, B.A. (2011). Intestinal stem cells in the adult Drosophila midgut. Experimental Cell Research *317*, 2780–2788.

Jiang, H., Edgar, B.A. (2009). EGFR signaling regulates the proliferation of Drosophila adult midgut progenitors. Development *136*, 483–493.

Jiang, H., Grenley, M.O., Bravo, M.J., Blumhagen, R.Z., Edgar, B.A. (2011). EGFR/Ras/MAPK Signaling Mediates Adult Midgut Epithelial Homeostasis and Regeneration in Drosophila. Stem Cell *8*, 84–95.

Jiang, H., Patel, P.H., Kohlmaier, A., Grenley, M.O., McEwen, D.G., Edgar, B.A. (2009). Cytokine/Jak/Stat signaling mediates regeneration and homeostasis in the Drosophila midgut. Cell *137*, 1343–1355.

Kapuria, S.S., Karpac, J.J., Biteau, B.B., Hwangbo, D.D., Jasper, H.H. (2012). Notch-mediated suppression of TSC2 expression regulates cell differentiation in the Drosophila intestinal stem cell lineage. PLoS Genet. *8*, e1003045–e1003045.

Klein, T.T., Campos-Ortega, J.A.J. (1997). klumpfuss, a Drosophila gene encoding a member of the EGR family of transcription factors, is involved in bristle and leg development. Development *124*, 3123–3134.

Liang, J., Balachandra, S., Ngo, S., O'Brien, L.E. (2017). Feedback regulation of steady-state epithelial turnover and organ size. Nature *548*, 588–591.

Lucchetta, E.M., Ohlstein, B. (2012). The Drosophila midgut: a model for stem cell driven tissue regeneration. Wiley Interdiscip Rev Dev Biol *1*, 781–788.

Meier, P., Silke, J., Leevers, S.J., Evan, G.I. (2000). The Drosophila caspase DRONC is regulated by DIAP1. The EMBO J. *19*, 598–611.

Micchelli, C.A., Perrimon, N. (2006). Evidence that stem cells reside in the adult Drosophila midgut epithelium. Nature *439*, 475–479.

Mollereau, B., Perez-Garijo, A., Bergmann, A., Miura, M., Gerlitz, O., Ryoo, H.D., Steller, H., Morata, G. (2012). Compensatory proliferation and apoptosis-induced proliferation: a need for clarification. Cell Death Differ. *20*, 181–181.

Notta, F., Zandi, S., Takayama, N., Dobson, S., Gan, O.I., Wilson, G., Kaufmann, K.B., McLeod, J., Laurenti, E., Dunant, C.F., McPherson, J.D., Stein, L.D., Dror, Y., Dick, J.E. (2016). Distinct routes of lineage development reshape the human blood hierarchy across ontogeny. Science *8*, 351(6269):aab2116

O'Brien, L.E., Soliman, S.S., Li, X., Bilder, D. (201)1. Altered modes of stem cell division drive adaptive intestinal growth. Cell *147*, 603–614.

Ohlstein, B., Spradling, A. (2007.) Multipotent Drosophila Intestinal Stem Cells Specify Daughter Cell Fates by Differential Notch Signaling. Science *315*, 988–992.

Ohlstein, B., Spradling, A. (2006). The adult Drosophila posterior midgut is maintained by pluripotent stem cells. Nature *439*, 470–474.

Parasram, K., Bernardon, N., Hammoud, M., Chang, H., He, L., Perrimon, N., Karpowicz, P. (2018). Intestinal Stem Cells Exhibit Conditional Circadian Clock Function. Stem Cell Peports *13*, 1287-1301.

Perdigoto, C.N., Schweisguth, F., Bardin, A.J. (2011). Distinct levels of Notch activity for commitment and terminal differentiation of stem cells in the adult fly intestine. Development *138*, 4585–4595.

Potten, C.S. (1992). The significance of spontaneous and induced apoptosis in the gastrointestinal tract of mice. Cancer Metast Rev *11*, 179–195.

Potten, C.S., Owen, G., Booth, D. (2002). Intestinal stem cells protect their genome by selective segregation of template DNA strands. J. Cell Sci. *115*, 2381–2388.

Protzer, C.E., Wech, I., Nagel, A.C. (2008). Hairless induces cell death by downregulation of EGFR signalling activity. J. Cell Sci. *12*1, 3167–3176.

Raff, M.C. (1996). Size control: the regulation of cell mumbers in animal development. Cell *86*, 173–175.

Rusconi, J.C., Fink, J.L., Cagan, R. (2004). klumpfuss regulates cell death in the Drosophila retina. Mech. Dev. *121*, 537–546.

Sallé, J., Gervais, L., Boumard, B., Stefanutti, M., Siudeja, K., Bardin, A.J., 2017. Intrinsic regulation of enteroendocrine fate by Numb. The EMBO J. 36, 1928–1945. doi:10.15252/embj.201695622

Siddall, N.A.N., Behan, K.J.K., Crew, J.R.J., Cheung, T.L.T., Fair, J.A.J., Batterham, P.P., Pollock, J.A.J., 2003. Mutations in lozenge and D-Pax2 invoke ectopic patterned cell death in the developing Drosophila eye using distinct mechanisms. Development Genes and Evolution 213, 107–119. doi:10.1007/s00427-003-0295-y

Simons, B.D., Clevers, H. (2011). Stem cell self-renewal in intestinal crypt. Exp. Cell Res. *317*, 2719–2724.

Vasudevan, D., Don Ryoo, H. (2015). Regulation of Cell Death by IAPs and Their Antagonists. Curr. Top Dev. Biol. *114*, 185–208.

Vaux, D.L., Korsmeyer, S.J. (1999). Cell Death in Development. Cell *96*, 245–254.

Wildonger, J. (2005). Lozenge directly activates argos and klumpfuss to regulate programmed cell death. Genes Dev. *19*, 1034–1039.

Zacharioudaki, E., Bray, S.J. (2014). Tools and methods for studying Notch signaling in Drosophila melanogaster. Methods *68*, 173–182.

Zeng, X., Hou, S.X. (2015). Enteroendocrine cells are generated from stem cells through a distinct progenitor in the adult Drosophila posterior midgut. Development 142, 644–653.

Zhai, Z., Kondo, S., Ha, N., Boquete, J.-P., Brunner, M., Ueda, R., Lemaitre, B. (2015). Accumulation of differentiating intestinal stem cell progenies drives tumorigenesis. Nat Comms *6*, 10219.

Zhang, L., Ren, F., Zhang, Q., Chen, Y., Wang, B., Jiang, J. (2008). The TEAD/TEF Family of Transcription Factor Scalloped Mediates Hippo Signaling in Organ Size Control. Dev. Cell *14*, 377–387.

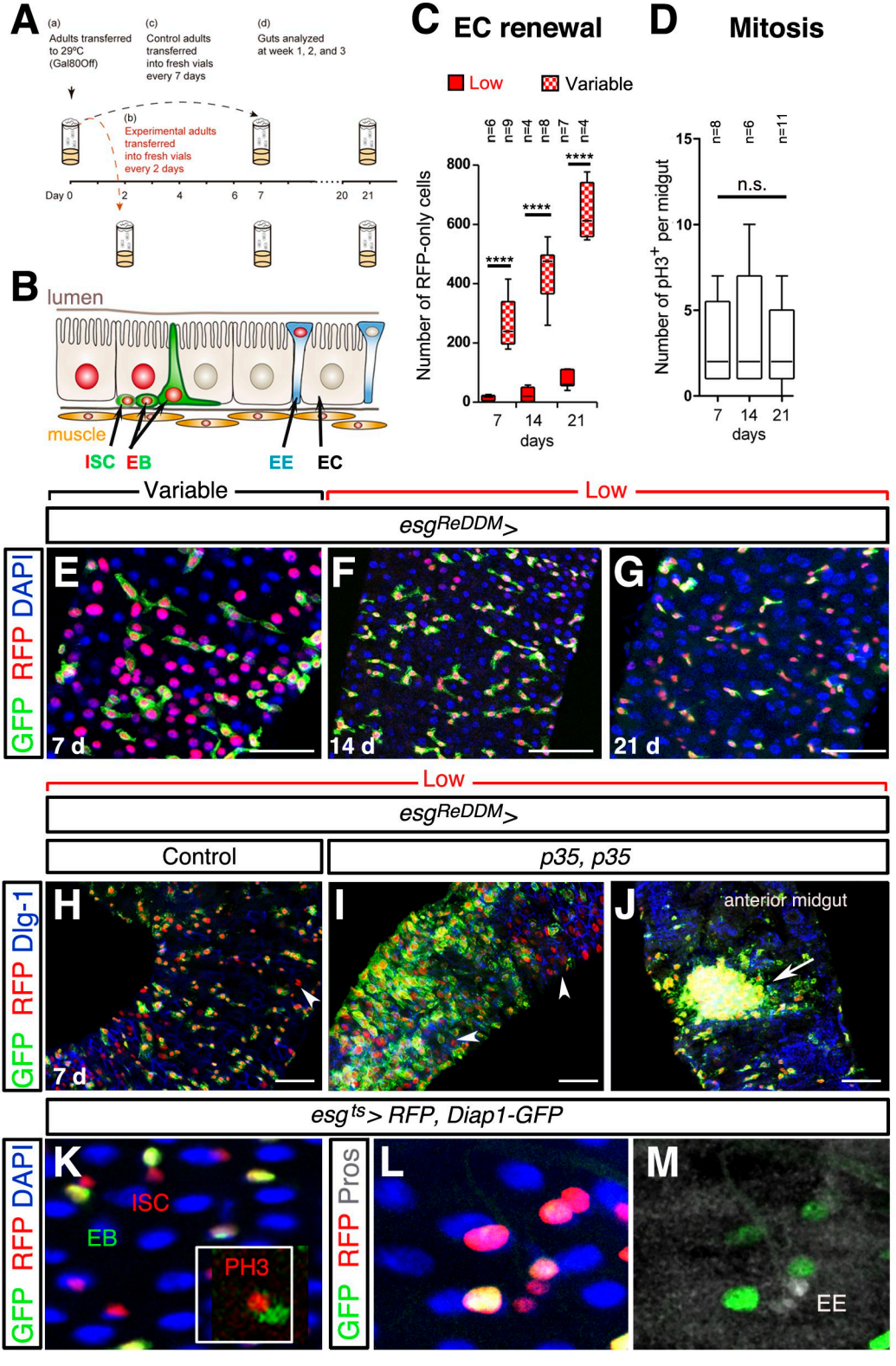

Figure 1 Reiff, Antonello et al

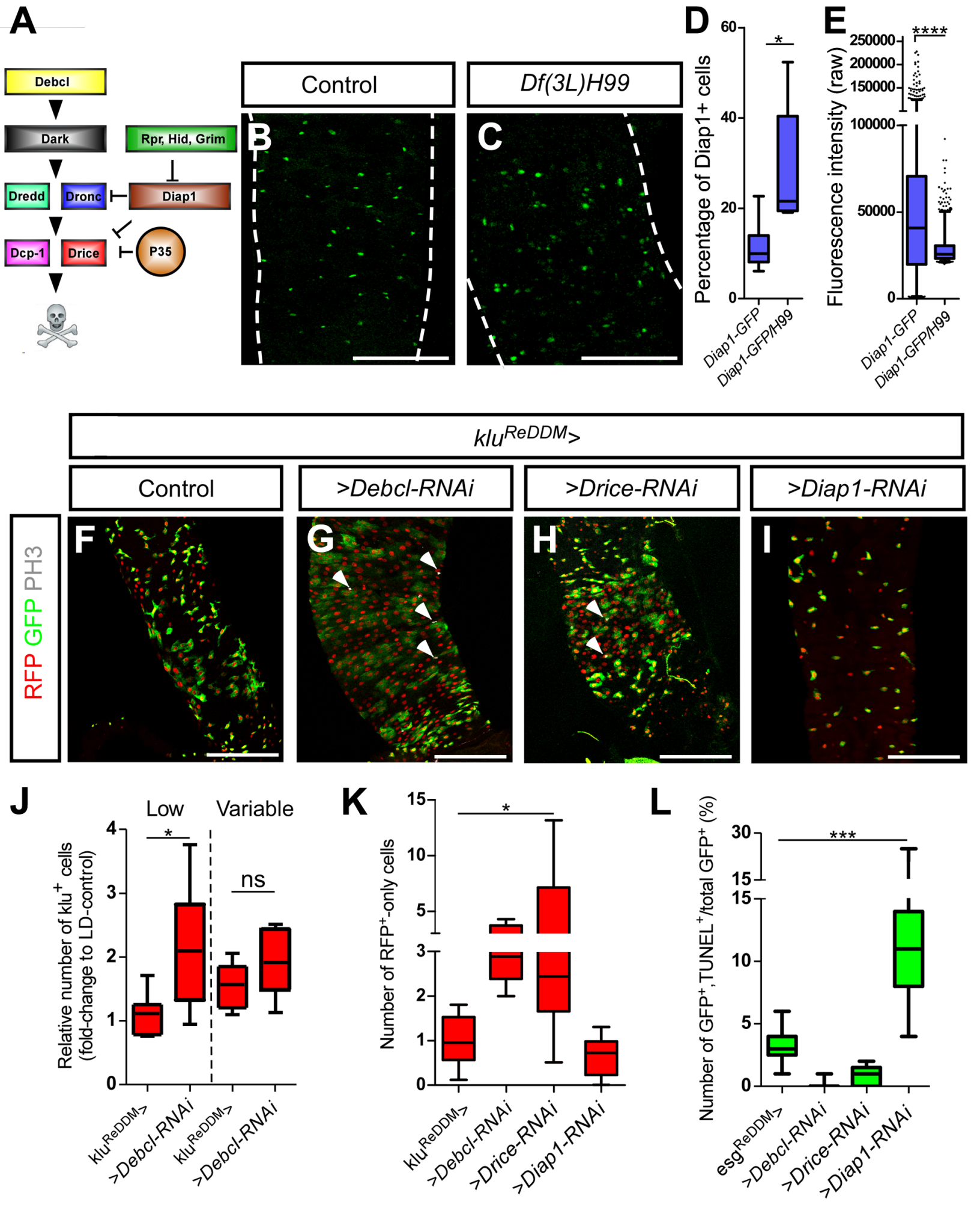
A
Debcl
Dark
Rpr, Hid, Grim
Dredd
Dronc
Diap1
Dcp-1
Drice
P35
Control
Df(3L)H99
B
C
D
Percentage of Diap1+ cells
60
40
20
0
*
Diap1-GFP
Diap1-GFP/H99
E
Fluorescence intensity (raw)
250000
200000
150000
100000
50000
0
****
Diap1-GFP
Diap1-GFP/H99
klu^ReDDM>
Control
>Debcl-RNAi
>Drice-RNAi
>Diap1-RNAi
RFP GFP PH3
F
G
H
I
J
Low
Variable
Relative number of klu+ cells
(fold-change to LD-control)
4
3
2
1
0
*
ns
kluReDDM>
>Debcl-RNAi
kluReDDM>
>Debcl-RNAi
K
Number of RFP+-only cells
15
10
5
3
2
1
0
*
kluReDDM>
>Debcl-RNAi
>Drice-RNAi
>Diap1-RNAi
L
Number of GFP+,TUNEL+/total GFP+ (%)
30
15
15
10
5
0
***
esgReDDM>
>Debcl-RNAi
>Drice-RNAi
>Diap1-RNAi

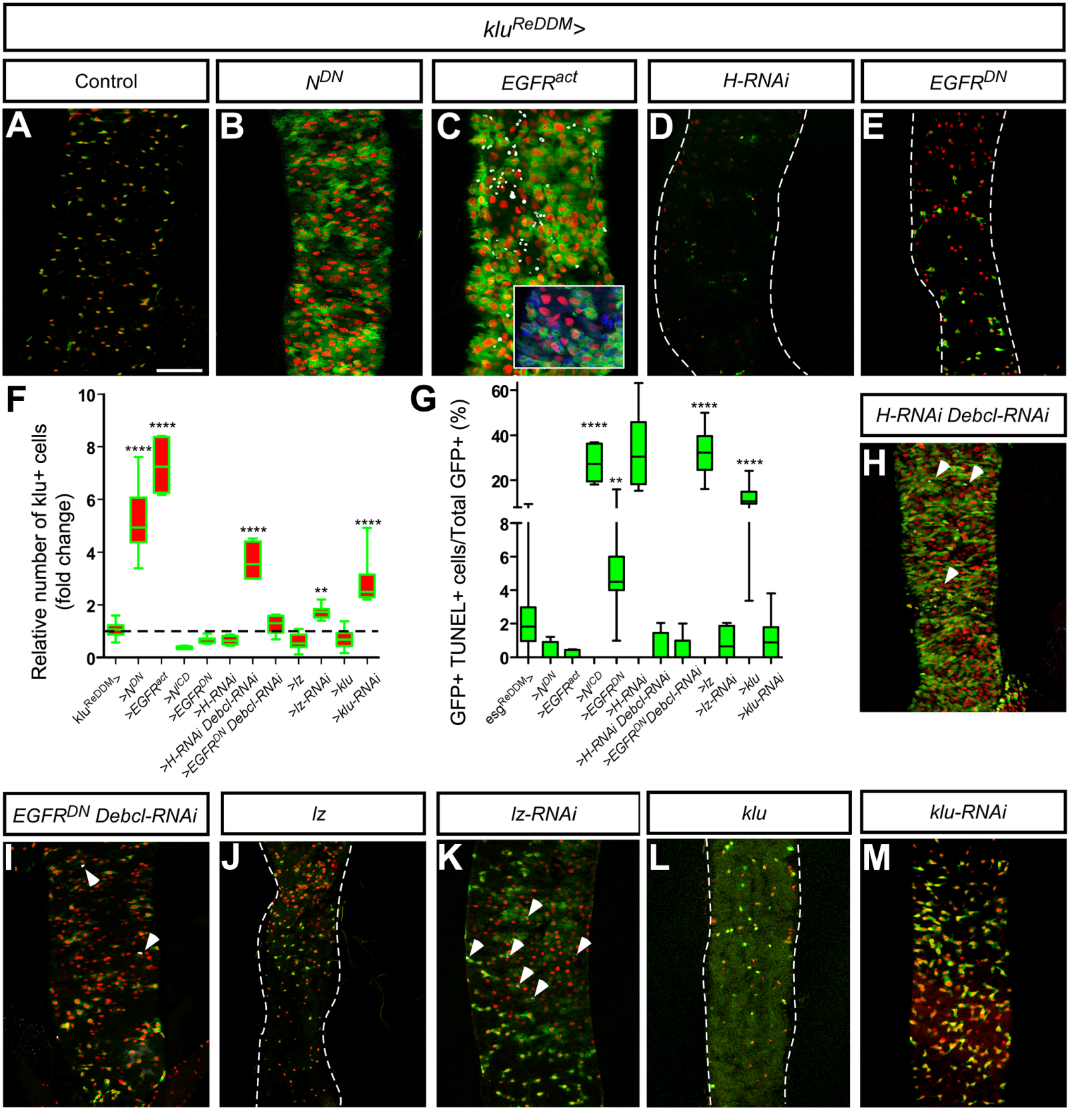
klu^ReDDM>
Control
N^DN
EGFR^act
H-RNAi
EGFR^DN
A
B
C
D
E
F
Relative number of klu+ cells (fold change)
klu^ReDDM>
>N^DN
>EGFR^act
>N^ICD
>EGFR^DN
>H-RNAi
>H-RNAi Debcl-RNAi
>EGFR^DN Debcl-RNAi
>lz
>lz-RNAi
>klu
>klu-RNAi
G
GFP+ TUNEL+ cells/Total GFP+ (%)
esg^ReDDM>
H-RNAi Debcl-RNAi
H
EGFR^DN Debcl-RNAi
lz
lz-RNAi
klu
klu-RNAi
I
J
K
L
M

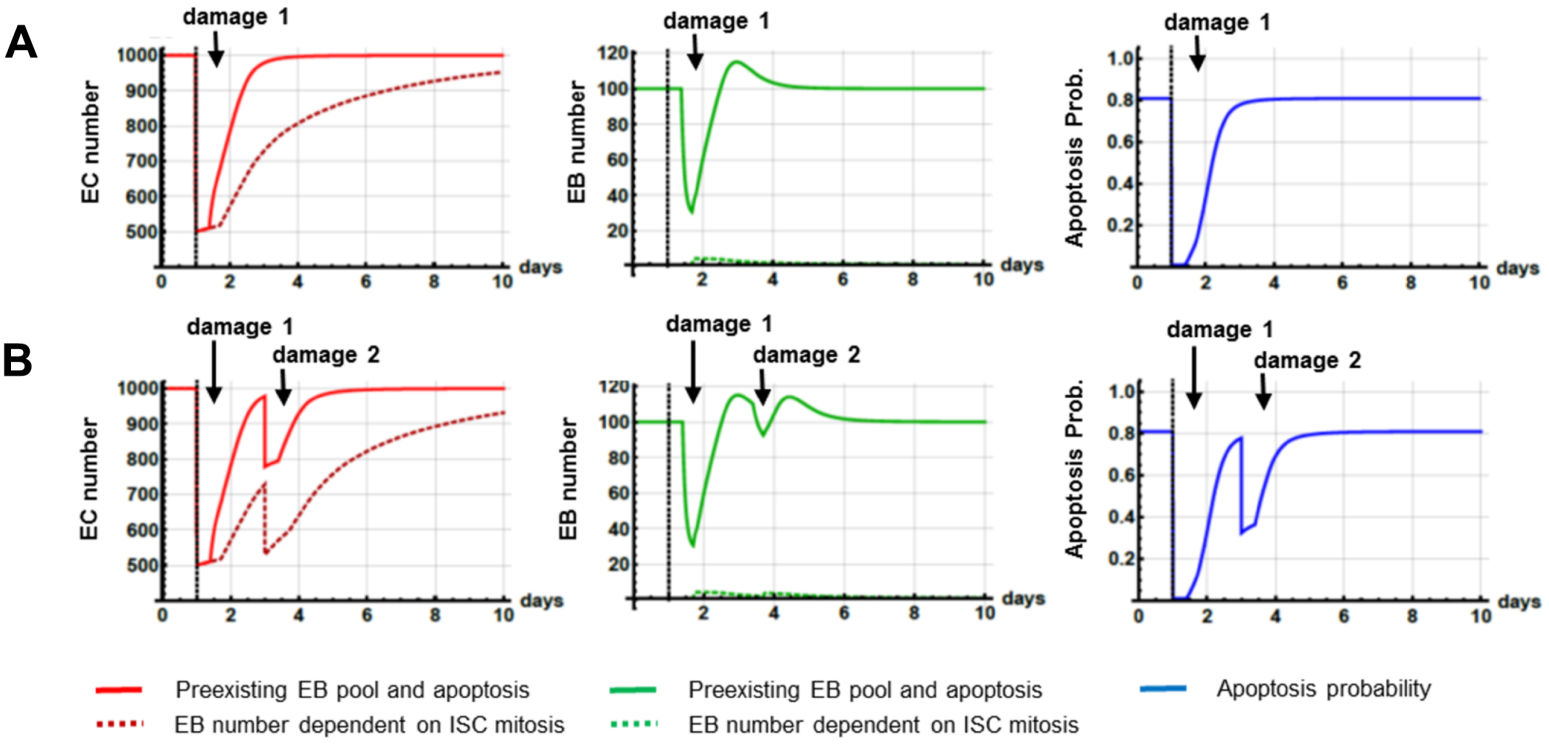
A
damage 1
EC number
EB number
Apoptosis Prob.
days
B
damage 1
damage 2
Preexisting EB pool and apoptosis
EB number dependent on ISC mitosis
Apoptosis probability

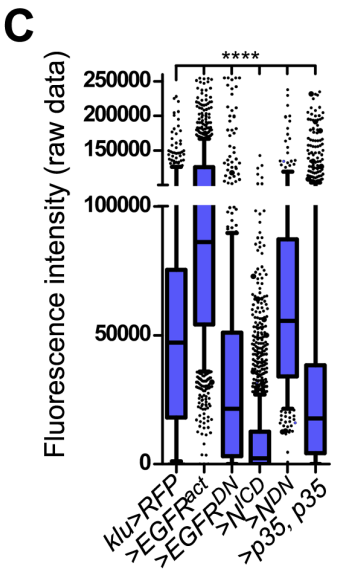
C
Fluorescence intensity (raw data)
klu>RFP
>EGFRact
>EGFRDN
>NICD
>NDN
>p35, p35

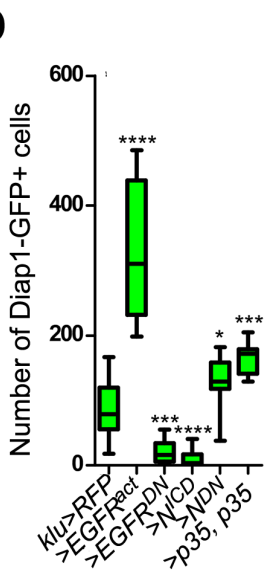
D
Number of Diap1-GFP+ cells

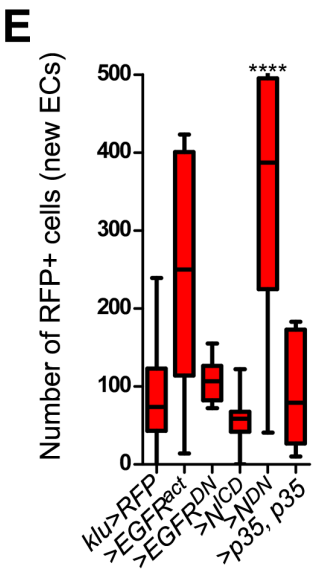
E
Number of RFP+ cells (new ECs)

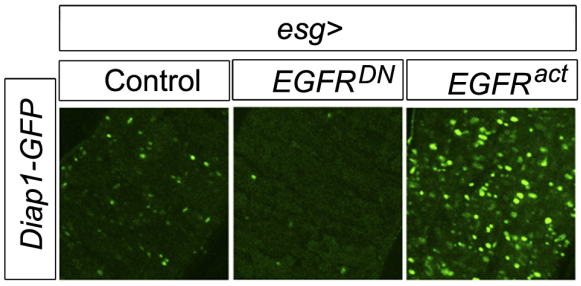
F
esg>
Control
EGFRDN
EGFRact
Diap1-GFP